
Task-Optimized Convolutional Recurrent Networks Align with Tactile Processing in the Rodent Brain

Trinity Chung^{*,1}, Yuchen Shen^{*,2}, Nathan C. L. Kong⁴, and Aran Nayebi^{2, 3, 1}

¹Robotics Institute, Carnegie Mellon University; Pittsburgh, PA 15213

²Machine Learning Department, Carnegie Mellon University; Pittsburgh, PA 15213

³Neuroscience Department, Carnegie Mellon University; Pittsburgh, PA 15213

⁴Department of Psychology, University of Pennsylvania; Philadelphia, PA 19104

* Equal contribution.

{trinityc, yuchens3, anayebi}@cs.cmu.edu; nclkong@sas.upenn.edu

Abstract

Tactile sensing remains far less understood in neuroscience and less effective in artificial systems compared to more mature modalities such as vision and language. We bridge these gaps by introducing a novel Encoder-Attender-Decoder (EAD) framework to systematically explore the space of task-optimized temporal neural networks trained on realistic tactile input sequences from a customized rodent whisker-array simulator. We identify convolutional recurrent neural networks (ConvRNNs) as superior encoders to purely feedforward and state-space architectures for tactile categorization. Crucially, these ConvRNN-encoder-based EAD models achieve neural representations closely matching rodent somatosensory cortex, saturating the explainable neural variability and revealing a clear linear relationship between supervised categorization performance and neural alignment. Furthermore, contrastive self-supervised ConvRNN-encoder-based EADs, trained with tactile-specific augmentations, match supervised neural fits, serving as an ethologically-relevant, label-free proxy.

For neuroscience, our findings highlight nonlinear recurrent processing as important for general-purpose tactile representations in somatosensory cortex, providing the first quantitative characterization of the underlying inductive biases in this system. For embodied AI, our results emphasize the importance of recurrent EAD architectures to handle realistic tactile inputs, along with tailored self-supervised learning methods for achieving robust tactile perception with the same type of sensors animals use to sense in unstructured environments.

1 Introduction

Humans and animals have remarkable abilities to interact with and interpret complex environments through active sensing, where tactile perception plays an essential role along with vision [Lederman and Klatzky, 2009]. Biological organisms effectively leverage tactile sensors, such as whiskers, to precisely navigate, forage, and identify objects even in noisy and unstructured conditions; specifically, contact whiskers deliver critical sensory input for navigation, foraging, and hunting in low-light environments [Ahl, 1986], while water-flow whiskers enable seals to discriminate prey movements from general water currents in similar conditions [Dehnhardt et al., 2001], and specialized insect hairs respond to wind stimuli, providing information essential for flight stability and agility [Sterbing-D’Angelo et al., 2011].

Rodents are a common model organism for studying tactile perception in the brain due to the fine experimental control they offer and their ability to discriminate object location, shape, and texture

using only their whiskers [Hires et al., 2015, Cheung et al., 2019]. These whiskers, or *vibrissae*, transmit rich mechanical signals to mechanoreceptors at their base, enabling nuanced environmental understanding without direct sensory receptors along their lengths. In fact, rodent whisking behavior is known to parallel how humans touch objects with their fingertips [Staiger and Petersen, 2021], such as in the Lateral Motion Exploratory Procedure [Lederman and Klatzky, 2009]. Despite significant interest in translating such biological capabilities into robots, artificial systems still struggle to match the tactile perceptual prowess of animals, limiting their functionality in realistic, unstructured environments [Navarro-Guerrero et al., 2023].

There are two primary reasons for this gap: one from the robotics hardware side, and the other from the neuroscience side. On the hardware side, current bio-inspired whisker sensors for robots face several critical limitations, including substantial hardware complexity when scaling sensor arrays beyond approximately 18–20 whiskers, each requiring individual transducers, significantly increasing wiring and computational demands [Pearson et al., 2011, Assaf et al., 2016]. These sensors also struggle to accurately discriminate multiple simultaneous stimuli such as airflow, direct contact, and inertia, unlike biological whiskers [Simon et al., 2023]. Additionally, mechanical discrepancies from biological whiskers—such as reduced sensitivity, limited flexibility, and constrained bending angles—impede precise tactile sensing in dynamic environments [Kent et al., 2023, Kent and Bergbreiter, 2024].

These limitations also apply to artificial hands, which remain in a relatively early stage of development. For example, besides not being able to sense temperature, good mechanical skin has remained an open challenge in haptics for approximately four decades, primarily due to difficulties in creating artificial skins that maintain realistic deformation during object contact, with current pneumatic approaches proving inadequate to retain shape [Shimonomura, 2019, Dahiya et al., 2009]. While depth-camera-based methods such as GelSight [Yuan et al., 2017] offer a limited haptic solution by providing localized surface height maps, they fundamentally differ from human tactile sensing, which actively integrates diverse mechanoreceptor inputs over larger surfaces and multiple contacts [Ward-Cherrier et al., 2018]. This issue persists with recent magnetic-based methods such as ReSkin [Bhirangi et al., 2021] and AnySkin [Bhirangi et al., 2024a], which, despite their richer force-based tactile representations, remain localized to small sensing surfaces and can be prone to sensor slippage [Bhirangi et al., 2024b]. These hardware limitations thus make it difficult at the moment to identify robust algorithms for tactile processing that operate on realistic sensory inputs.

Concurrently, from the neuroscience side, despite extensive experimental characterization of rodent somatosensory pathways (e.g. [Armstrong-James et al., 1992, Kerr et al., 2007]), the neural computations underlying precise tactile perception remain poorly understood, primarily due to a scarcity of computational models of this system. Rodent whisker sensing involves hierarchical processing, analogous to vision, where sensory signals propagate from primary neurons in the trigeminal ganglion through parallel thalamic pathways, eventually reaching the primary and secondary somatosensory cortices (S1 and S2) [Bosman et al., 2011, Moore et al., 2015]. However, relatively few computational approaches have explicitly modeled these neural transformations [Zhuang et al., 2017], and none have assessed if any of these models accurately match neural population responses in somatosensory cortex.

To bridge these gaps, we build and systematically evaluate temporal neural networks explicitly trained on biomechanically-realistic force and torque tactile sequences that mice receive, customized from the first complete 3D simulation of the rat’s whisker array by Zweifel et al. [2021]. We identify convolutional recurrent neural networks (ConvRNNs), particularly IntersectionRNNs, as superior in tactile categorization and neural alignment compared to feedforward (ResNet) and attention-based state-space models (S4 and Mamba). Leveraging supervised and contrastive self-supervised learning adapted specifically for tactile data, we demonstrate a direct linear relationship between tactile categorization performance and neural fit, saturating the currently explainable neural variability and surpassing inter-animal consistency benchmarks, with contrastive self-supervised learning serving as an equally neurally predictive, label-free proxy. Thus, we provide the *first* quantitative characterization of inductive biases required for tactile algorithms to match brain processing.

2 Related Work

Task-optimized neural network models have emerged as currently the most quantitatively accurate framework for understanding brain function. Such goal-driven modeling first successfully explained neural responses in primate visual areas across hierarchical stages [Yamins et al., Khaligh-Razavi and Kriegeskorte, 2014], and subsequently, auditory [Kell* et al., 2018, Feather et al., 2019], motor [Sussillo et al., Michaels et al.], memory [Nayebi et al., 2021], and language [Schrumpf et al., 2021] brain areas. While many of these results are in humans and non-human primates, goal-driven modeling approaches have more recently been extended to mouse visual cortex, demonstrating that shallow architectures trained via contrastive self-supervised learning best capture mouse visual cortical representations [Nayebi* et al., 2023, Bakhtiari et al., 2021].

Despite these advances, goal-driven computational modeling has not yet been extensively applied to tactile processing, even though tactile sensory systems share hierarchical and recurrent processing features with vision [Felleman and Van Essen, 1991]. Zhuang et al. [2017] provided a foundational goal-driven modeling approach for the rodent whisker-trigeminal system, yet their exploration was limited to relatively simple recurrent architectures and solely supervised categorization loss functions, and they did not compare their models to brain data. Here, we significantly broaden the architectural exploration via a novel Encoder-Attender-Decoder parametrization. We incorporate sophisticated convolutional RNN (“ConvRNN”) architectures previously developed by Nayebi* et al. [2018], which were shown to match primate visual cortex dynamics. Additionally, we explore advanced temporal models such as State Space Models (SSMs) (e.g. S4 [Gu et al., 2021] and Mamba [Gu and Dao, 2023]), and Transformers [Haldar et al., 2024]. We also employ self-supervised loss functions validated in mouse [Nayebi* et al., 2023, Bakhtiari et al., 2021] and primate visual cortex [Zhuang et al., 2021], adapted to specifically deal with force and torque inputs. Finally, we provide the first direct neural comparison to rodent somatosensory cortical responses across all 62 models.

3 Methods

High-variation tactile dataset generation with a biomechanical whisker simulator. Given the ongoing development of tactile sensor hardware to match the flexibility of biological tactile sensors such as fingertips and whiskers, we trained our models on synthetic data, focusing on object categorization and self-supervised learning using a high-variation dataset like ShapeNet [Chang et al., 2015]. This involves the simulated objects interacting with a biomechanically-realistic rodent whisker model, WHISKiT Physics [Zweifel et al., 2021], to provide high-dimensional force and torque inputs, constituting the first 3D simulation of the rodent’s complete whisker system, which models each of the 30 33 whiskers of an average whisker array [Belli et al., 2017, 2018] as a chain of 20 rigid

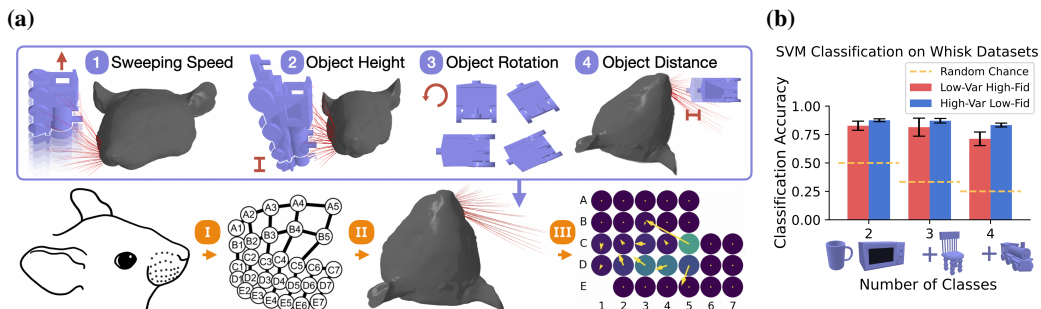


Figure 1: **ShapeNet Whisking Dataset.** (a) (I) With average mouse whisker array measurements from Bresee et al. [2023], (II) objects are whisked in simulation using WHISKiT [Zweifel et al., 2021] resulting in (III) force and torque data for sweeping 9981 ShapeNet objects of 117 categories with various sweep augmentations. The augmentations vary the (1) speed, (2) height, (3), rotation, and (4) distance of the objects relative to the whisker array. We constructed two datasets: a large, low-fidelity set with more sweep augmentations, and a small, high-fidelity set with fewer augmentations (see appendix). (b) An SVM classification on up to 4 different classes of objects (cups, microwaves, chairs, and trains) for the 2 datasets show that the classes are distinguishable (above chance).

conical segments interconnected by torsional springs and actuated according to established equations of motion [Knutson et al., 2008].

Since we will eventually compare with recently collected mouse somatosensory data [Rodgers, 2022], we adapted this array to the 30 whiskers of the mouse [Bresee et al., 2023], forming a 5×7 array with zero padding. Furthermore, adult mice can exhibit maximal bite forces of approximately 8-10 Newtons [Freeman and Lemen, 2008, Table 1], and since facial tolerance to applied forces would realistically be a fraction of this maximal bite force, our chosen simulation clipping range of ± 1000 milli-Newton (± 1 N) remains comfortably within biologically plausible limits.

For dataset generation, we focused on passive whisking, where the objects brush by the array in order to generate a high-variation dataset by which to strongly constrain the representations that are learned, allowing us to more effectively simulate evolutionary pressures, in line with the “Contravariance Principle” [Cao and Yamins, 2024] of goal-driven modeling. Namely, the higher variation and more ethologically-relevant the dataset is, the less the number of solutions that can effectively solve the task, leading to a higher probability of model-brain representational alignment. On each of the 9981 different objects from ShapeNet, we apply several combinations of sweep augmentations, including adjusting the object sweeping speed, height, rotation, and distance relative to the whisker array (Fig. 1). The 117 object categories are selected based on the work of Zhuang et al. [2017] to ensure reasonably distinguishable classes. We constructed two datasets: one large dataset replicating the Zhuang et al. [2017] data with 288 randomized sweep augmentations and a physics simulation step rate of 110 Hz (High-Variation/Low-Fidelity), and another with 16 sweep augmentations and a higher simulation step rate of 1000 Hz (Low-Variation/High-Fidelity). See the Appendix for detailed sweep augmentation procedures. Although higher temporal resolution is available from the simulation, we extract 22 timesteps for both datasets, corresponding to the average whisking frequency of 20 Hz in rodents [Sofroniew and Svoboda, 2015].

Encoder-Attender-Decoder (EAD) temporal model search parametrization. Tactile recognition is performed by the somatosensory cortex, which, though less understood than vision, exhibits hierarchical processing and long-range feedback connections [Lederman and Klatzky, 2009, Navarro-Guerrero et al., 2023]. These basic anatomical insights motivate our exploration of hierarchical, temporal neural network (TNN) models such as ConvRNNs shown previously to match primate visual cortex dynamics [Nayebi* et al., 2018, Nayebi et al., 2022], SSMs [Gu et al., 2021], Transformers [Haldar et al., 2024], and ResNets [He et al., 2016] as a feedforward control. As a result, we developed a new PyTorch library (“PyTorchTNN”) that enables large-scale exploration of integrating multiple TNN modules that additionally are combined by long-range feedback with feedforward connections.

These considerations produce a rather large search space of model architectures. Therefore, to be able to effectively search the space of TNN models systematically, we came up with an encoder-attender-decoder (EAD) parametrization, schematized in Fig. 2a. Convolutional recurrent and state-space layers (such as ConvRNNs and S4) are particularly effective for encoding smooth and compressible temporal signals, given their recurrent smoothing properties and linear-time complexity. In contrast, Transformers and other attention-like architectures (e.g., Mamba) excel at processing temporally sparse or irregularly informative inputs, as they independently weight each timestep. Given that the tactile inputs from force and torque sensors provide temporally smooth signals, the encoder (**E**) layers closer to these inputs naturally benefit from convolutional and recurrent mechanisms that integrate information locally over time, effectively reducing redundancy and noise. In contrast, higher-level temporal aggregation (**A**), which must selectively integrate meaningful signals across longer and potentially irregular timescales, is better served by attention-based architectures like Transformers or Mamba, which can dynamically weigh distinct timesteps based on their informational content. Finally, the decoder (**D**) is either the classification layer for supervised learning, or similarly producing self-supervised features for contrastive learning or autoencoding. Our EAD paradigm thus flexibly combines these complementary modules, enabling an effective and structured exploration of the temporal model space for tactile processing.

Specifically, we explore the following EAD combinations (visualized in Fig. 2a): 1) encoder: Zhuang’s recurrent model [Zhuang et al., 2017], ResNet [He et al., 2016], S4 [Gu et al., 2021]; 2) attender: Transformer [Haldar et al., 2024] (e.g., GPT), Mamba [Gu and Dao, 2023], None (i.e., attender-free); 3) decoder: MLP. We further investigate different variants of Zhuang’s model by replacing the recurrent layers in the ConvRNNs with UGRNN [Collins et al., 2017], Intersection-RNN [Collins et al., 2017], LSTM [Hochreiter and Schmidhuber, 1997], and GRU [Cho et al., 2014].

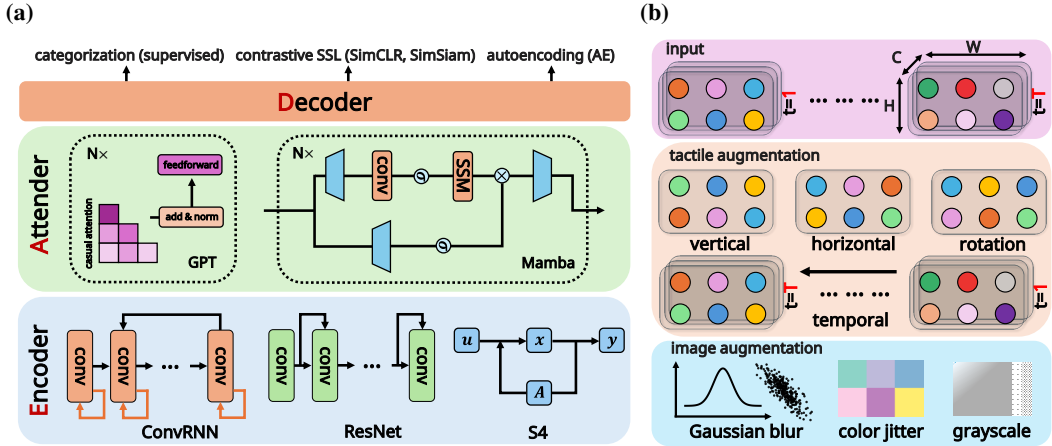


Figure 2: (a) **Encoder-Attender-Decoder (EAD)** architecture, with task objectives being supervised categorization, self-supervised learning (SimCLR, SimSiam), and autoencoding (AE). The ConvRNN encoder includes **self-recurrence** at each layer where we vary different RNNs.

(b) Types of data augmentations applied to SSL models. Given a temporal **tactile input** over time T , our **tactile augmentation** vertically, horizontally, temporally flips, and rotates the features, while traditional **image augmentation** introduces Gaussian noise, color jitter, and grayscale.

With the help of our PyTorchTNN library, each time step in the ConvRNNs corresponds to a single feedforward layer processing its input and passing it to the next layer, in contrast of treating each entire feedforward pass from input to output as one integral time step, as is normally done with RNNs [Spoerer et al., 2017].

Model Training and Tactile Augmentations. Besides the supervised categorization objective, we also consider self-supervised learning (SSL) losses: SimCLR [Chen et al., 2020], which learns robust representations via distinguishing the embeddings of augmentations of one image from other images, SimSiam [Chen and He, 2021], which maximizes the similarity between the embeddings of two augmentations of the same image, and autoencoding (AE) [Olshausen and Field, 1996], where we use a 3-layer deconvolution network to reconstruct an image from its sparse latent representation.

We use a train/validation/test split of 80%/10%/10%, and report the top-5 test accuracy. For supervised learning, we train models for 100 epochs and test on the checkpoint saved with the highest validation accuracy. For SSL objectives, we train for 100 epochs and save the model with the lowest validation loss, then continue training for another 100 epochs with the checkpoint frozen and a learnable linear layer on top of it. To stabilize training, we also consider adding layer norm [Ba et al., 2016] to the ConvRNNs as an alternative when training was unstable. All experiments are conducted on Nvidia A6000 GPUs, and one set of model search experiment takes 8~16 hours.

We illustrate the tactile input, our tactile augmentation, and traditional image augmentations for SSL in Fig. 2b. Given a temporal tactile input over time T , the proposed augmentation either vertically, horizontally flips, rotates the features, or reverses the input over time. Our tactile augmentation mimics flipping, rotation, and reverse-direction active whisking for tactile simulation; meanwhile, traditional image augmentations add noise, color jitter, and gray scale to the features, which fail to provide meaningful augmentations to tactile representation learning.

Neural Data Comparison. We use the neural dataset from Rodgers [2022], which recorded neural population activity from the superficial (L2/3) to deep (L6) layers of the barrel cortex of mice during an active whisking task involving object classification. After filtering for valid trials, the neural data we used contains a total of 999 neural units across 11 mice. The time window of each trial is clipped to the time of first whisker contact with the object until the time the mouse makes its decision (about 1-2 seconds). The neural response is binned into intervals of approximately 45–50 ms, corresponding neatly with the 15–20 Hz whisking frequency typical of rodents (50 ms per cycle at 20 Hz [Sofroniew and Svoboda, 2015]), and aligning specifically with our model’s integration scheme of five subtimesteps (~9 ms each) per timestep. This choice provides a temporal resolution optimal for capturing detailed neural activity during whisker-object contact periods.

We evaluate neural alignment using Representational Similarity Analysis (RSA), a parameter-free approach that compares the pairwise dissimilarity structure of model and neural population responses across the same set of stimuli. RSA compares the pairwise dissimilarity structure of neural responses and model activations to a common set of stimuli, allowing direct comparison of representational geometry without requiring additional parameter fitting [Kriegeskorte et al., 2008].

To ensure only reliable neurons are included, we compute split-half internal consistency of the neural responses across trials and retain only neurons with a Spearman-Brown-corrected reliability greater than 0.5. All RSA evaluations are thus conducted on this filtered subset of self-consistent neurons, and corrected by this internal consistency. For more details about this procedure, please consult the Appendix.

The noise-corrected RSA Pearson’s r score is also computed between one mouse to every other mouse, and then averaged this score across all mice to obtain the mean animal score which will serve as the baseline for model-brain evaluation, to account for inherent animal-to-animal variability (which we denote as “a2a” in the barplots). Thus, we want our models to match the brain, at least as well as animals do to each other.

Next, we replicated the experimental setup of the barrel cortex dataset Rodgers [2022] *in silico*. Fig. 4a shows the 6 different stimuli used in the experiment, which are concave/convex objects at three different distances (near, medium, far) from the whisker array. With 3D model reproduction of the concave/convex objects in the experiment, active whisking is simulated under the 6 stimuli using a real recorded whisking trajectory [Bresee et al., 2023] to generate the model input.

We then obtain the neural alignment score for models by computing the maximum, across all layers, of the median RSA score between each layer’s representation and the neural responses, averaged across mice. The standard error is calculated across the RSA Pearson’s r value from the model to each mouse.

4 Results

Validation of Sensor and Dataset via SVM Decoding. We first verified the basic discriminability of the whisker array dataset using support vector machine (SVM) classifiers on the High-Variation/Low-Fidelity and Low-Variation/High-Fidelity datasets (Fig. 1b). Both showed strong decoding performance, exceeding chance and remaining robust even with increased task difficulty from more object categories. The comparable results across sampling rates confirm that the smaller 1000 Hz dataset retains sufficient discriminative tactile information, allowing for efficient model training without compromising performance.

ConvRNN Encoders Outperform Feedforward and Attention-based Architectures for Tactile Categorization. We next systematically evaluated the task performance of the EAD architectures trained on biomechanically-realistic force and torque tactile sequences. Overall, we found that across EAD architectures, the choice of encoder (E) was quite important for tactile recognition. Specifically, ConvRNN encoders, especially the IntersectionRNN [Collins et al., 2017], surpassed the purely feedforward ResNet18 and SSM (S4) encoders, in supervised tactile categorization tasks (Fig. 3). Additionally, models trained with our custom force-and-torque-specific contrastive self-supervised learning (SSL) augmentations (Fig. 2b) outperformed untrained networks of the same architecture, and those trained with standard image-based augmentations that involve Gaussian blur and color jittering [Chen et al., 2020] did not train with the best architecture despite hyperparameter tuning,

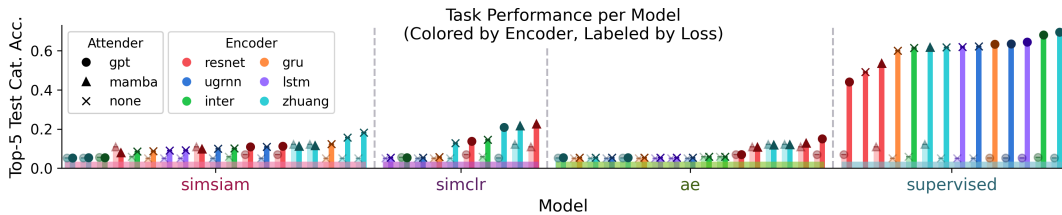


Figure 3: **Tactile Categorization Accuracy.** The lighter-colored left bar represents the randomly initialized version for every model. The best-performing model is Zhuang+GPT+Supervised (rightmost cyan bar).

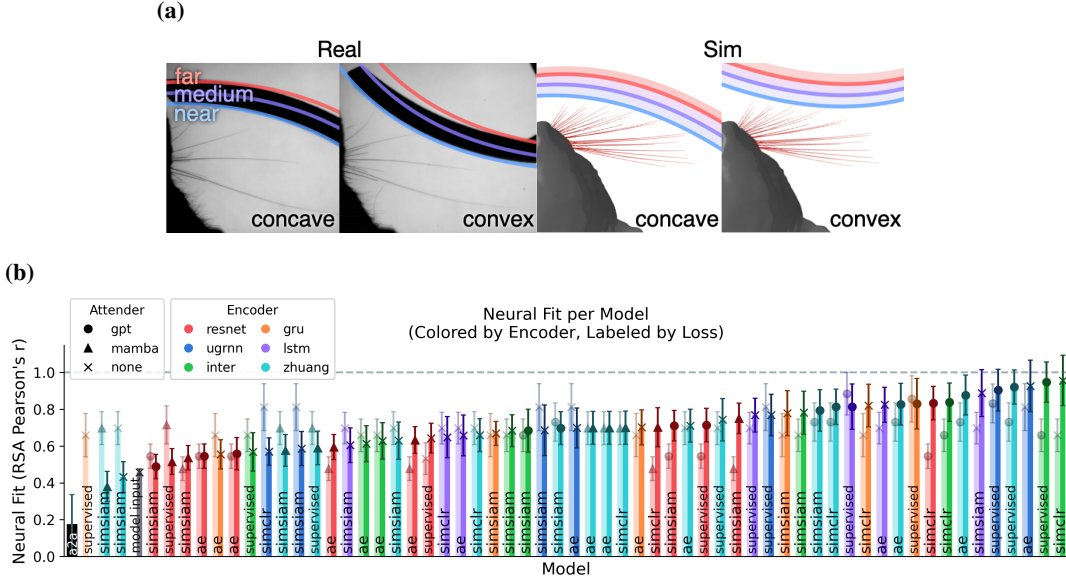


Figure 4: **Model Neural Evaluation.** (a) We use six different stimuli (concave/convex \times near/medium/far) replicating the conditions in the mouse neural dataset in simulation. (Real images were taken from video recordings in neural dataset [Rodgers, 2022]). (b) Comparison of neural fit (noise-corrected RSA Pearson’s r) across models. The mean animal-to-animal score is 0.18 and the maximum between all pairs of animals is 1.16. The leftmost “a2a” bar represents the *mean* animal-to-animal neural consistency score. The lighter-colored left bar represents the randomly initialized version for every model.

demonstrating the importance of tailored tactile augmentations for enhancing task performance (Fig. 3).

ConvRNN Encoders Saturate Explainable Neural Variance in Rodent Somatosensory Cortex. To assess biological realism, we compared internal model representations to neural recordings from rodent whisker somatosensory cortex. All trained EAD models outperformed raw sensor inputs in neural alignment, underscoring the importance of nonlinear temporal processing in modeling brain-like tactile representations (Fig. 4b). In fact, the best models saturated *all* of the held-out explainable neural variance—*without* fitting any additional parameters—even when tested on entirely novel objects under substantially different experimental conditions (active whisker sensing rather than passive contact, as used in training). Remarkably, the neural predictivity exceeded the average inter-animal neural consistency (leftmost black “a2a” bar in Fig. 4b), thereby robustly passing the NeuroAI Turing Test on this dataset [Feather* et al., 2025]. Among these and consistent with the categorization results, EAD models with ConvRNN encoders consistently provided better neural fits compared to feedforward (ResNet) and SSM-based (S4) encoder architectures, underscoring the biological plausibility of recurrence in modeling tactile processing. In fact, we saw a strong linear trend between tactile supervised categorization performance and neural fit ($r = 0.59$, Fig. 5b), with the model layers that best predict the tactile neural responses being closest to the decoder layer (Fig. A2). While the number of task-optimized parameters matters for both categorization test set performance and neural fit generalization (Fig. A1), they are not the whole story, as the SimCLR-trained EAD with the IntersectionRNN encoder, best matches the neural data with far less parameters ($\sim 3.80 \times 10^7$ parameters) than its supervised counterpart with a GPT-based attender ($\sim 6.38 \times 10^7$ parameters).

GPT-based Attenders Provide Modest Improvements in Task Performance and Neural Alignment. In addition to varying the encoder (E) layer of the EADs, we investigated different temporal aggregation (“Attender”) schemas. We observed that GPT-based Attenders modestly outperformed Mamba-based and no-attention controls in both supervised task categorization and neural alignment (Fig. 5b). Although these improvements were subtle, the consistency of the result suggests that incorporating some form of attention downstream of the ConvRNN encoder is beneficial, particularly for our highest-performing neural models. This result suggests the prediction that attention-like mechanisms may be implemented in somatosensory cortex through selective modulation of hierarchical processing pathways, such as those from primary sensory neurons in the trigeminal ganglion

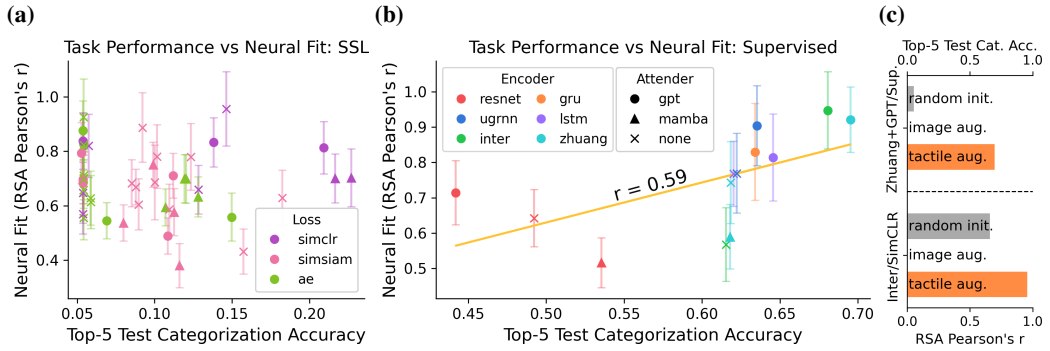


Figure 5: **Comparing Task Performance and Neural Fit.** (a) The task performance of SSL models are about one order of magnitude below the performance of supervised models, yet are able to achieve comparable neural fit. (b) For supervised models, we observe a trend of better task performance leading to increased neural correspondence. Plotting a best fit line, we find the correlation $r = 0.59$. (c) The tactile augmentations were effective in improving both the neural fit and task performance. The models were unable to be trained with image augmentations.

through the thalamus and subsequently into primary and secondary somatosensory cortical areas (S1 and S2), which could be validated by experiments involving targeted perturbations or optogenetic manipulation of these specific pathways during tactile discrimination tasks.

Self-Supervised SimCLR Training Matches Supervised Models and Serves as an Ethologically-Relevant Label-Free Proxy. We compared neural alignment achieved by supervised training against SSL methods, adapted with tactile-specific force-and-torque augmentations. This comparison is necessary because discriminating among 117 human-recognizable shape classes is not directly ethologically relevant for rodents. Nevertheless, ShapeNet’s extensive diversity of 3D objects provides strong structural constraints for modeling whisker-trigeminal processing at biological scales, constraints which smaller, mouse-relevant object sets might fail to impose. Paralleling findings in vision [Yamins et al., Khaligh-Razavi and Kriegeskorte, 2014], where training on large-scale object categorization leads to generalizable representations beyond specific categories, we similarly suggest that ShapeNet’s diversity provides meaningful constraints on network structure irrespective of exact object identity. Additionally, by demonstrating that self-supervised learning (SSL) methods yield neural representations comparable (if not marginally better) to supervised approaches, we directly address an open direction highlighted by Zhuang et al. [2017], who emphasized the need for developing more ethologically relevant yet practically scalable tasks for studying tactile processing.

In fact, we found specifically that *contrastive* SSL loss functions consistently reached neural alignment scores similar to the best supervised models, confirming its utility as an ethologically-relevant but label-free approach to tactile representation learning (Fig. 5a), and outperforming other *non-contrastive* self-supervised approaches such as autoencoding. The SimCLR-optimized Intersection-RNN EAD achieved the best absolute neural alignment score across all models overall, and was comparable in its neural alignment to its supervised (and more parameter-dense) variant (rightmost green bars in Fig. 4b). This result mirrors findings in primate visual cortex [Zhuang et al., 2021], where contrastive SSL methods equally predicted neural response patterns compared to supervised alternatives, suggesting supervised learning serves as a proxy for this more ethologically-relevant loss function. Interestingly, the parity between contrastive SSL and supervised models observed here differs from mouse visual cortex, where contrastive SSL methods substantially exceeded supervised methods in neural predictivity [Nayebi* et al., 2023]. Notably, the SSL methods, which are best aligned with tactile neural representations overall, achieve only moderate linear probe categorization performance (Fig. 5a), implying that somatosensory cortex representations might prioritize broader, task-agnostic sensory encoding rather than purely specialized, categorization-driven features. Furthermore, just as we found for downstream task performance in Fig. 3, we also observed it was critical to have tactile-specific SSL augmentations for developing biologically accurate tactile representations, compared to both standard image-based SimCLR augmentations and randomly initialized architecture-fixed controls (Fig. 5c).

5 Discussion

Implications for Somatosensory Cortical Processing. We developed a novel Encoder-Attender-Decoder (EAD) parametrization of the space of temporal neural network models (TNN) trained to perform tactile recognition on biomechanically-realistic force and torque sequences, greatly extending and answering the open question posed by Zhuang et al. [2017] of characterizing the ethologically-relevant constraints of rodent whisker-based tactile computations. Our results establish ConvRNN encoders, particularly the IntersectionRNN, as currently superior in tactile categorization performance and neural representational alignment compared to feedforward (ResNet) and state-space models (SSM), suggesting recurrent processing is more relevant overall to the rodent somatosensory system. Furthermore, we demonstrated that contrastive self-supervised learning (SimCLR), particularly when trained with tactile-specific augmentations, yields neural alignments comparable to supervised methods, highlighting supervised training as a proxy for a more ethologically relevant, label-free representation. The modest yet consistent benefits observed from GPT-based Attenders indicate potential attention-like mechanisms operating within hierarchical tactile processing pathways, suggesting a fruitful avenue for experimental validation.

Taken together, our findings indicate that nonlinear recurrent processing play an essential role in the rodent somatosensory cortex, reflecting neural encoding strategies that prioritize broad, general-purpose tactile representations. This work provides the first quantitative characterization of the inductive biases required for tactile algorithms to match brain processing, opening new opportunities for deeper insights into sensory representation learning and somatosensory cortical dynamics.

Implications for Embodied AI and Robotics. Current artificial tactile sensors and models fall short of animal-like capabilities, limiting the functional use of robots in real-world, unstructured scenarios. Our results underscore the importance of biomechanically-realistic inputs and temporally recurrent EAD architectures for developing tactile perception models that perceive touch similarly as animals do. Our demonstration that tactile-specific (force and torque) SSL augmentations significantly enhance performance underscores this point, emphasizing the necessity of tailored training methods for robotic tactile systems. Future work in embodied robotic systems leveraging these insights could potentially overcome existing sensor limitations, including scaling complexity, stimulus discrimination challenges, and restricted sensing surfaces, thereby achieving more robust and nuanced environmental interactions akin to biological organisms.

Limitations and Future Directions. Our findings represent not the final word, but rather the beginning of an improved understanding of tactile sensory processing in both animals and machines. Most importantly, current tactile neural datasets remain limited in stimulus diversity and the number of object conditions tested, restricting the captured neural variability and could be the reason why inter-animal consistency values are lower for the statistical average between animals than the current pointwise empirical maximum of 1.4 (Fig. 4b), indicated by the NeuroAI Turing Test. Expanding neural datasets to include broader sets of tactile stimuli and additional animals will thus be crucial for future work, enabling models to approach and potentially surpass this theoretical ceiling of neural predictivity.

In the longer term, incorporating multimodal sensory integration will be important—particularly combining tactile inputs with other modalities, such as proprioception or vision, through biologically-inspired fusion operations that integrate signals extensively across intermediate layers, as is observed in the brain [Navarro-Guerrero et al., 2023], rather than relying solely on last-layer concatenation, as is commonly done now [Yang et al., 2024]. Exploring precisely (1) where and (2) how these multimodal signals are best fused, using diverse fusion operations (e.g., concatenation, attention, routing), is already supported by our PyTorchTNN library and will yield stronger constraints on models, potentially enabling more robust tactile-driven decision-making in genuinely unstructured scenarios as well as animals do.

Broader Impacts. Improving robotic tactile sensing to not only match human *capabilities*, but also quantitatively validating, as we explicitly do, shared processing of object properties with human collaborators at the level of *internal* representations, could enhance human safety and efficiency in environments such as healthcare, assistive technologies, and manufacturing in the future. However, advancements in tactile-enabled robotics might also disrupt employment in sectors relying heavily on manual labor. It will therefore be important to thoughtfully manage these technological transitions through proactive policy-making and workforce training.

6 Acknowledgements

We thank Albert Gu and Roberta “Bobby” Klatzky for helpful discussions. A.N. thanks the Burroughs Wellcome Fund and Google Robotics Award for funding.

References

A. S. Ahl. The role of vibrissae in behavior: a status review. *Veterinary research communications*, 10(1):245–268, 1986.

M. Armstrong-James, K. Fox, and A. Das-Gupta. Flow of excitation within rat barrel cortex on striking a single vibrissa. *Journal of neurophysiology*, 68(4):1345–1358, 1992.

T. Assaf, E. D. Wilson, S. Anderson, P. Dean, J. Porritt, and M. J. Pearson. Visual-tactile sensory map calibration of a biomimetic whiskered robot. In *2016 IEEE International Conference on Robotics and Automation (ICRA)*, pages 967–972. IEEE, 2016.

J. L. Ba, J. R. Kiros, and G. E. Hinton. Layer normalization, 2016. URL <https://arxiv.org/abs/1607.06450>.

S. Bakhtiari, P. Mineault, T. Lillicrap, C. Pack, and B. Richards. The functional specialization of visual cortex emerges from training parallel pathways with self-supervised predictive learning. *Advances in Neural Information Processing Systems*, 34:25164–25178, 2021.

H. M. Belli, A. E. Yang, C. S. Bresee, and M. J. Hartmann. Variations in vibrissal geometry across the rat mystacial pad: base diameter, medulla, and taper. *Journal of Neurophysiology*, 117(4):1807–1820, 2017.

H. M. Belli, C. S. Bresee, M. M. Graff, and M. J. Hartmann. Quantifying the three-dimensional facial morphology of the laboratory rat with a focus on the vibrissae. *PLoS One*, 13(4):e0194981, 2018.

R. Bhirangi, T. Hellebrekers, C. Majidi, and A. Gupta. Reskin: versatile, replaceable, lasting tactile skins. *arXiv preprint arXiv:2111.00071*, 2021.

R. Bhirangi, V. Pattabiraman, E. Erciyes, Y. Cao, T. Hellebrekers, and L. Pinto. Anyskin: Plug-and-play skin sensing for robotic touch. *arXiv preprint arXiv:2409.08276*, 2024a.

R. Bhirangi, C. Wang, V. Pattabiraman, C. Majidi, A. Gupta, T. Hellebrekers, and L. Pinto. Hierarchical state space models for continuous sequence-to-sequence modeling. *arXiv preprint arXiv:2402.10211*, 2024b.

L. W. Bosman, A. R. Houweling, C. B. Owens, N. Tanke, O. T. Shevchouk, N. Rahmati, W. H. Teunissen, C. Ju, W. Gong, S. K. Koekkoek, et al. Anatomical pathways involved in generating and sensing rhythmic whisker movements. *Frontiers in integrative neuroscience*, 5:53, 2011.

L. Bottou. Large-scale machine learning with stochastic gradient descent. In *Proceedings of COMPSTAT'2010: 19th International Conference on Computational StatisticsParis France, August 22-27, 2010 Keynote, Invited and Contributed Papers*, pages 177–186. Springer, 2010.

C. S. Bresee, H. M. Belli, Y. Luo, and M. J. Z. Hartmann. Comparative morphology of the whiskers and faces of mice (*mus musculus*) and rats (*rattus norvegicus*). *Journal of Experimental Biology*, 226(19):jeb245597, 10 2023. ISSN 0022-0949. doi: 10.1242/jeb.245597. URL <https://doi.org/10.1242/jeb.245597>.

R. Cao and D. Yamins. Explanatory models in neuroscience, part 2: Functional intelligibility and the contravariance principle. *Cognitive Systems Research*, 85:101200, 2024.

A. X. Chang, T. Funkhouser, L. Guibas, P. Hanrahan, Q. Huang, Z. Li, S. Savarese, M. Savva, S. Song, H. Su, et al. Shapenet: An information-rich 3d model repository. *arXiv preprint arXiv:1512.03012*, 2015.

T. Chen, S. Kornblith, M. Norouzi, and G. Hinton. A simple framework for contrastive learning of visual representations. In *International conference on machine learning*, pages 1597–1607. PMLR, 2020.

X. Chen and K. He. Exploring simple siamese representation learning. In *Proceedings of the IEEE/CVF conference on computer vision and pattern recognition*, pages 15750–15758, 2021.

J. Cheung, P. Maire, J. Kim, J. Sy, and S. A. Hires. The sensorimotor basis of whisker-guided anteroposterior object localization in head-fixed mice. *Current Biology*, 29(18):3029–3040, 2019.

K. Cho, B. van Merriënboer, C. Gulcehre, D. Bahdanau, F. Bougares, H. Schwenk, and Y. Bengio. Learning phrase representations using rnn encoder-decoder for statistical machine translation, 2014. URL <https://arxiv.org/abs/1406.1078>.

J. Collins, J. Sohl-Dickstein, and D. Sussillo. Capacity and trainability in recurrent neural networks. In *ICLR*, 2017.

E. Coumans and Y. Bai. Pybullet, a python module for physics simulation for games, robotics and machine learning. <http://pybullet.org>, 2016–2021.

R. S. Dahiya, G. Metta, M. Valle, and G. Sandini. Tactile sensing—from humans to humanoids. *IEEE transactions on robotics*, 26(1):1–20, 2009.

G. Dehnhardt, B. Mauck, W. Hanke, and H. Bleckmann. Hydrodynamic trail-following in harbor seals (*phoca vitulina*). *Science*, 293(5527):102–104, 2001.

J. Feather, A. Durango, R. Gonzalez, and J. McDermott. Metamers of neural networks reveal divergence from human perceptual systems. In *Advances in Neural Information Processing Systems*, pages 10078–10089, 2019.

J. Feather*, M. Khosla*, N. Murty*, and A. Nayebi*. Brain-model evaluations need the neuroai turing test. *arXiv preprint arXiv:2502.16238*, 2025.

D. J. Felleman and D. C. Van Essen. Distributed hierarchical processing in the primate cerebral cortex. *Cerebral cortex (New York, NY: 1991)*, 1(1):1–47, 1991.

P. W. Freeman and C. A. Lemen. A simple morphological predictor of bite force in rodents. *Journal of Zoology*, 275(4):418–422, 2008.

A. Gu and T. Dao. Mamba: Linear-time sequence modeling with selective state spaces. *arXiv preprint arXiv:2312.00752*, 2023.

A. Gu, K. Goel, and C. Ré. Efficiently modeling long sequences with structured state spaces. *arXiv preprint arXiv:2111.00396*, 2021.

S. Haldar, Z. Peng, and L. Pinto. Baku: An efficient transformer for multi-task policy learning. *arXiv preprint arXiv:2406.07539*, 2024.

K. He, X. Zhang, S. Ren, and J. Sun. Deep residual learning for image recognition. In *Proceedings of the IEEE conference on computer vision and pattern recognition*, pages 770–778, 2016.

S. A. Hires, D. A. Gutnisky, J. Yu, D. H. O’Connor, and K. Svoboda. Low-noise encoding of active touch by layer 4 in the somatosensory cortex. *elife*, 4:e06619, 2015.

S. Hochreiter and J. Schmidhuber. Long short-term memory. *Neural Computation*, 9(8):1735–1780, 1997.

A. J. Kell*, D. L. Yamins*, E. N. Shook, S. V. Norman-Haigere, and J. H. McDermott. A task-optimized neural network replicates human auditory behavior, predicts brain responses, and reveals a cortical processing hierarchy. *Neuron*, 98(3):630–644, 2018.

T. A. Kent and S. Bergbreiter. Flow shadowing: A method to detect multiple flow headings using an array of densely packed whisker-inspired sensors. In *2024 IEEE International Conference on Robotics and Automation (ICRA)*, pages 17843–17849. IEEE, 2024.

T. A. Kent, H. Emmett, M. Babaei, M. J. Hartmann, and S. Bergbreiter. Identifying contact distance uncertainty in whisker sensing with tapered, flexible whiskers. In *2023 IEEE International Conference on Robotics and Automation (ICRA)*, pages 607–613. IEEE, 2023.

J. N. Kerr, C. P. De Kock, D. S. Greenberg, R. M. Bruno, B. Sakmann, and F. Helmchen. Spatial organization of neuronal population responses in layer 2/3 of rat barrel cortex. *Journal of neuroscience*, 27(48):13316–13328, 2007.

S.-M. Khaligh-Razavi and N. Kriegeskorte. Deep supervised, but not unsupervised, models may explain it cortical representation. *PLoS computational biology*, 10(11):e1003915, 2014.

D. P. Kingma and J. Ba. Adam: A method for stochastic optimization. In *ICLR*, 2015.

P. M. Knutsen, A. Biess, and E. Ahissar. Vibrissal kinematics in 3d: tight coupling of azimuth, elevation, and torsion across different whisking modes. *Neuron*, 59(1):35–42, 2008.

N. Kriegeskorte, M. Mur, and P. A. Bandettini. Representational similarity analysis-connecting the branches of systems neuroscience. *Frontiers in systems neuroscience*, 2:249, 2008.

S. J. Lederman and R. L. Klatzky. Haptic perception: A tutorial. *Attention, Perception, & Psychophysics*, 71(7):1439–1459, 2009.

I. Loshchilov and F. Hutter. Decoupled weight decay regularization, 2019. URL <https://arxiv.org/abs/1711.05101>.

K. Mamou and F. Ghorbel. A simple and efficient approach for 3d mesh approximate convex decomposition. pages 3501–3504, 11 2009. doi: 10.1109/ICIP.2009.5414068.

J. A. Michaels, S. Schaffelhofer, A. Aguadé-Toro, and H. Scherberger. A goal-driven modular neural network predicts parietofrontal neural dynamics during grasping. 117(50):32124–32135.

J. D. Moore, N. Mercer Lindsay, M. Deschênes, and D. Kleinfeld. Vibrissa self-motion and touch are reliably encoded along the same somatosensory pathway from brainstem through thalamus. *PLoS biology*, 13(9):e1002253, 2015.

N. Navarro-Guerrero, S. Toprak, J. Josifovski, and L. Jamone. Visuo-haptic object perception for robots: an overview. *Autonomous Robots*, 47(4):377–403, 2023.

A. Nayebi*, D. Bear*, J. Kubilius*, K. Kar, S. Ganguli, D. Sussillo, J. J. DiCarlo, and D. L. Yamins. Task-driven convolutional recurrent models of the visual system. In S. Bengio, H. Wallach, H. Larochelle, K. Grauman, N. Cesa-Bianchi, and R. Garnett, editors, *Advances in Neural Information Processing Systems*, volume 31. Curran Associates, Inc., 2018.

A. Nayebi, A. Attinger, M. Campbell, K. Hardcastle, I. Low, C. Mallory, G. Mel, B. Sorscher, A. Williams, S. Ganguli, L. M. Giocomo, and D. L. Yamins. Explaining heterogeneity in medial entorhinal cortex with task-driven neural networks. *Advances in Neural Information Processing Systems*, 34, 2021.

A. Nayebi, J. Sagastuy-Brena, D. M. Bear, K. Kar, J. Kubilius, S. Ganguli, D. Sussillo, J. J. DiCarlo, and D. L. Yamins. Recurrent connections in the primate ventral visual stream mediate a tradeoff between task performance and network size during core object recognition. *Neural Computation*, 34:1652–1675, 2022.

A. Nayebi*, N. C. Kong*, C. Zhuang, J. L. Gardner, A. M. Norcia, and D. L. Yamins. Mouse visual cortex as a limited resource system that self-learns an ecologically-general representation. *PLOS Computational Biology*, 19, 2023.

B. A. Olshausen and D. J. Field. Emergence of simple-cell receptive field properties by learning a sparse code for natural images. *Nature*, 381(6583):607–609, 1996.

M. J. Pearson, B. Mitchinson, J. C. Sullivan, A. G. Pipe, and T. J. Prescott. Biomimetic vibrissal sensing for robots. *Philosophical Transactions of the Royal Society B: Biological Sciences*, 366(1581):3085–3096, 2011.

C. C. Rodgers. A detailed behavioral, videographic, and neural dataset on object recognition in mice. *Scientific Data*, 9(1):620, 2022.

M. Schrimpf, I. A. Blank, G. Tuckute, C. Kauf, E. A. Hosseini, N. Kanwisher, J. B. Tenenbaum, and E. Fedorenko. The neural architecture of language: Integrative modeling converges on predictive processing. *Proceedings of the National Academy of Sciences*, 118(45):e2105646118, 2021.

K. Shimonomura. Tactile image sensors employing camera: A review. *Sensors*, 19(18):3933, 2019.

N. Simon, A. Z. Ren, A. Piqué, D. Snyder, D. Barretto, M. Hultmark, and A. Majumdar. Flowdrone: wind estimation and gust rejection on uavs using fast-response hot-wire flow sensors. In *2023 IEEE International Conference on Robotics and Automation (ICRA)*, pages 5393–5399. IEEE, 2023.

N. J. Sofroniew and K. Svoboda. Whisking. *Current Biology*, 25(4):R137–R140, 2015.

C. J. Spoerer, P. McClure, and N. Kriegeskorte. Recurrent convolutional neural networks: a better model of biological object recognition. *Front. Psychol.*, 8:1–14, 2017.

J. F. Staiger and C. C. Petersen. Neuronal circuits in barrel cortex for whisker sensory perception. *Physiological reviews*, 101(1):353–415, 2021.

S. Sterbing-D’Angelo, M. Chadha, C. Chiu, B. Falk, W. Xian, J. Barcelo, J. M. Zook, and C. F. Moss. Bat wing sensors support flight control. *Proceedings of the National Academy of Sciences*, 108(27):11291–11296, 2011.

D. Sussillo, M. M. Churchland, M. T. Kaufman, and K. V. Shenoy. A neural network that finds a naturalistic solution for the production of muscle activity. 18(7):1025–1033.

B. Ward-Cherrier, N. Pestell, L. Cramphorn, B. Winstone, M. E. Giannaccini, J. Rossiter, and N. F. Lepora. The tactip family: Soft optical tactile sensors with 3d-printed biomimetic morphologies. *Soft robotics*, 5(2): 216–227, 2018.

D. L. Yamins, H. Hong, C. F. Cadieu, E. A. Solomon, D. Seibert, and J. J. DiCarlo. Performance-optimized hierarchical models predict neural responses in higher visual cortex. 111(23):8619–8624.

F. Yang, C. Feng, Z. Chen, H. Park, D. Wang, Y. Dou, Z. Zeng, X. Chen, R. Gangopadhyay, A. Owens, et al. Binding touch to everything: Learning unified multimodal tactile representations. In *Proceedings of the IEEE/CVF Conference on Computer Vision and Pattern Recognition*, pages 26340–26353, 2024.

Y. You, I. Gitman, and B. Ginsburg. Large batch training of convolutional networks.

W. Yuan, S. Dong, and E. H. Adelson. Gelsight: High-resolution robot tactile sensors for estimating geometry and force. *Sensors*, 17(12):2762, 2017.

C. Zhuang, J. Kubilius, M. J. Hartmann, and D. L. Yamins. Toward goal-driven neural network models for the rodent whisker-trigeminal system. *Advances in Neural Information Processing Systems*, 30, 2017.

C. Zhuang, S. Yan, A. Nayebi, M. Schrimpf, M. C. Frank, J. J. DiCarlo, and D. L. Yamins. Unsupervised neural network models of the ventral visual stream. *Proceedings of the National Academy of Sciences*, 118(3), 2021.

N. O. Zweifel, N. E. Bush, I. Abraham, T. D. Murphey, and M. J. Hartmann. A dynamical model for generating synthetic data to quantify active tactile sensing behavior in the rat. *Proceedings of the National Academy of Sciences*, 118(27):e2011905118, 2021.

Appendix

A1 Whisk Dataset Generation

Our whisking dataset uses the same 9981 ShapeNet objects and 117 category labels as in Zhuang et al. [2017], but using an improved whisker model and various sweep augmentations, which are listed in Table 1.

	Sim. Freq.	Speed	Height	Rotation	Distance	Size	Total Sweeps
(1)	1000 Hz	30 mm/s [30~60]	-5, 0 mm -3, 0, 3	0, 30, 90, 120° [0~359]	5, 8 mm 5	40 mm [20~60]	316,192 2,076,048
(2)	110 Hz						

Table 1: **Sweep Augmentations** used for the two whisking datasets, which we refer to as (1) Low-Variation High-Fidelity and (2) High-Variation Low-Fidelity. Simulation Frequency refers to the frequency corresponding to the physics timestep used in Bullet physics engine [Coulmans and Bai, 2016–2021], the backend for WHISKiT simulator [Zweifel et al., 2021]. For dataset (2), the speed, rotation, and size is each sampled from the range 26 times. The total number of sweeps equals the number of sweep augmentation combinations \times 9981 objects.

WHISKiT Simulator Modifications. We make a few enhancements to the original WHISKiT simulator [Zweifel et al., 2021], available in our code:

- Number of whisker links (where whiskers are modeled as a chain of springs [Zhuang et al., 2017]) are dynamically adjusted by the length of the whisker instead of a fixed number.
- Allow for loading objects with or without convex hull. In the whisk datasets, objects are loaded with convex hull (using V-HACD [Mamou and Ghorbel, 2009]) to keep collisions more stable. In generating the 6 simulated stimuli for model input neural evaluation, convex hull was not used in order to preserve the concavity of the “concave” object. The object was geometrically simple enough to not affect collision stability.
- Add camera settings for viewing in orthographic or perspective projection.
- Load multiple mice/rats at a time.

A2 Model Training

All of our experiments are conducted on Nvidia A6000 GPUs. For supervised learning, we use a batch size of 256 for all the models and train for 100 epochs. For SSL, during the pre-training stage, we use a batch size of 256 for SimCLR and autoencoding (AE), and a batch size of 1024 for SimSiam, following Nayebi* et al. [2023], and train for 100 epochs. During the linear probing stage, we freeze the checkpoint saved with the lowest validation loss and add a trainable linear layer. We further train such a model with labels for 100 epochs, with a batch size of 256, an initial learning rate of 0.1, with the StepLR scheduler, and the SGD optimizer with momentum [Bottou, 2010].

We detail the optimizers [Bottou, 2010, Kingma and Ba, 2015, Loshchilov and Hutter, 2019, You et al.] and schedulers, and their configurations we used in supervised learning and SSL in Table 2.

For supervised learning, we present the model training configurations in Table 3, where we detail the choices of optimizer, scheduler, learning rate, the encoder and attender of our EAD architecture, and we omit the decoder due to space limits, as it is always a linear layer/MLP. As Zhuang+GPT is the best performing supervised model in terms of classification accuracy, we explore different variants of Zhuang’s encoder with attender being GPT.

For SSL, we follow Nayebi* et al. [2023] and use specific configurations of optimizer and scheduler for different losses, which are shown in Table 4. For SimSiam, we try the CosineAnnealing scheduler both with and without 10 epochs of warmup to search for better model performance. For AE, we use a 3-layer deconvolution network to decode the sparse latent representation from our EAD framework into the original tactile input, regardless of the choice of model architectures.

We present the model architectures explored for SSL in Table 5, where we present the encoder and attender of our EAD architecture, as during the pre-training stage, only the encoder and attender are used, and during the linear probing stage, the decoder is always a one-layer linear classification head.

Optimizer	Configuration
SGD	<code>momentum = 0.9, weight-decay = 10⁻⁴</code>
Adam	<code>weight-decay = 10⁻⁴</code>
AdamW	<code>weight-decay = 10⁻⁴</code>
LARS	<code>momentum = 0.9, weight-decay = 10⁻⁴</code>
Scheduler	Configuration
StepLR	<code>step_size = 30</code>
ConstantLR	<code>fixed learning rate</code>
CosineLR	<code>warmup_epoch = 10</code>
CosineAnnealing	<code>min_lr = 0.0, warmup_epoch = 10</code> <code>warmup_ratio = 10⁻⁴</code>

Table 2: **Optimizers and Schedulers** with default configurations of supervised learning and SSL when training different model architectures.

Encoder	Attender	Optimizer	Scheduler	Learning Rate
ResNet	None	SGD	StepLR	$10^{\{-1, -2, -3\}}$
Zhuang	None	SGD	StepLR	$10^{\{-1, -2, -3, -4\}}$
		SGD	ConstantLR	$10^{-2}, 5 \times 10^{-3}$
Zhuang-{UGRNN, IntersectionRNN, GRU, LSTM}	None	{SGD, Adam, AdamW}	StepLR	$10^{\{-1, -2, -3, -4\}}$
		(LayerNorm) - AdamW	StepLR	$10^{\{-1, -2, -3, -4\}}$
{ResNet, Zhuang, Zhuang-{UGRNN, IntersectionRNN-LN, GRU, LSTM}, S4}	GPT	AdamW	CosineLR	10^{-4}
		{SGD, AdamW}	StepLR	$10^{\{-1, -2, -3\}}$
{ResNet, Zhuang, S4}	Mamba	AdamW	CosineLR	10^{-4}
		{SGD, AdamW}	StepLR	$10^{\{-1, -2, -3\}}$

Table 3: **Model Training Configurations for Supervised Learning**. We use {} to indicate different choices of a specific component (i.e., encoder, optimizer, learning rate) in the search space. We consider adding layer norm as a variant when searching the best configuration for Zhuang’s variants (i.e., the second row), which is denoted as “-LN”.

A3 Neural Evaluation

We use the NeuroAI Turing Test [Feather* et al., 2025] to evaluate the neural similarity of mice whisking to models performing tactile categorization.

RSA Correlation. Due to the low number of stimuli, we use RSA [Kriegeskorte et al., 2008] as our correlation metric. RSA is computed over stimuli and neurons, where the average is over source animals/subsampled source neurons, bootstrapped trials, and train/test splits. This yields a vector of these average values, which we can take median and s.e.m. over, across animals.

For the neurons of animal A to animal B in the set of animals \mathcal{A} we estimate the RSA correlation:

$$\langle \text{RSA}(t^A, t^B) \rangle_{A \in \mathcal{A}: (A, B) \in \mathcal{A} \times \mathcal{A}} \sim \left\langle \frac{\text{RSA}(s_1^A, s_2^B)}{\sqrt{\text{RSA}(s_1^A, s_2^A) \times \text{RSA}(s_1^B, s_2^B)}} \right\rangle_{A \in \mathcal{A}: (A, B) \in \mathcal{A} \times \mathcal{A}}. \quad (1)$$

We additionally bootstrap across trials, and have all 50%/50% train/test splits ($\binom{6}{3} = 20$ splits). The average on the right hand side of the equation includes averages across these as well. Each neuron in our analysis is associated with this average value when it was a target animal (B), averaged over source animals or subsampled source neurons, bootstrapped trials, and train/test splits. This yields a vector of these average values, which we can take median and standard error of the mean (s.e.m.) over, as we do with standard explained variance metrics.

Spearman-Brown Correction. The Spearman-Brown correction can be applied to each of the terms in the denominator individually, as they are each correlations of observations from half the trials of

Loss	Optimizer	Scheduler	Learning Rate
SimCLR	LARS	CosineAnnealing	$10\{-1, -2, -3, -4\}$
SimSiam	SGD	CosineAnnealing (with & w/o warmup)	$10\{-1, -2, -3, -4\}$
AE	SGD	StepLR	$10\{-1, -2, -3, -4\}$

Table 4: **Optimizer, Scheduler, and Learning Rate Configurations for SSL** when training different model architectures.

Encoder	Attender
Zhuang	None
Zhuang-{UGRNN, IntersectionRNN-LN, GRU, LSTM}	None
{ResNet, Zhuang-IntersectionRNN-LN, Zhuang, S4}	GPT
{ResNet, Zhuang, S4}	Mamba

Table 5: **Model Architecture Configurations for SSL**. We use {} to indicate different choices of encoders in the search space. We consider adding layer norm (LN) as a variant when searching the best configuration for Zhuang’s variants (i.e., the second row)

the *same* underlying process to itself (unlike the numerator).

$$\begin{aligned} \widetilde{\text{RSA}}(X, Y) &:= \widetilde{\text{Corr}}(\text{RDM}(x), \text{RDM}(y)) \\ &= \frac{2 \text{RSA}(X, Y)}{1 + \text{RSA}(X, Y)}. \end{aligned}$$

Inter-Animal Consistency. To estimate the inter-animal consistency, we evaluate the pooled animal consistency for each animal. One animal is held out at a time, then compared to the pseudo-population aggregated across units from the remaining animals. We found the mean pooled animal score was 0.175 with a s.e.m. of 0.161 and maximum score of 1.34.

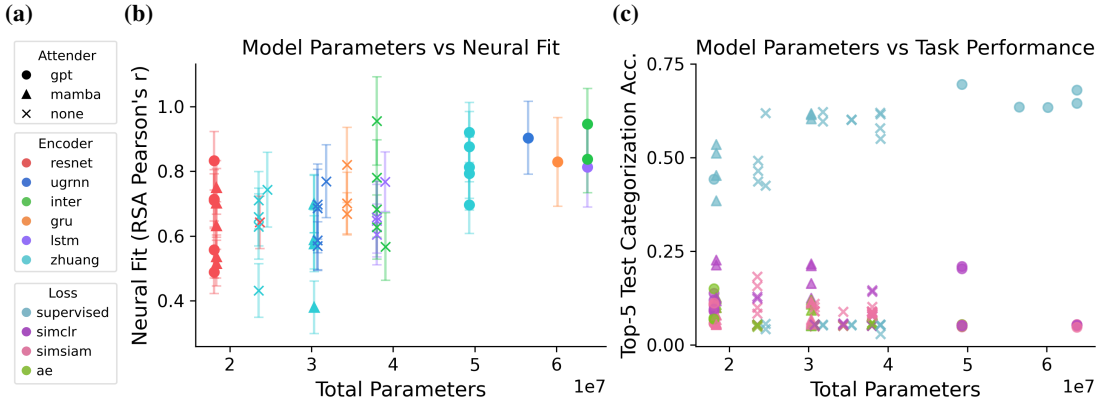


Figure A1: **Model Parameters** compared with categorization performance and neural fit. (a) Legends for (b) (Encoder colors) and (c) (Loss colors). (b) Models with GPT as an attender have a higher correlation score slightly higher than those without, but high neural fit is still achievable without more parameters as demonstrated by the Inter+SimCLR model (high green “ \times ”). (c) Models with GPT as the attender has more parameters and, when trained with supervised learning, tends to have higher top-5 categorization accuracy.

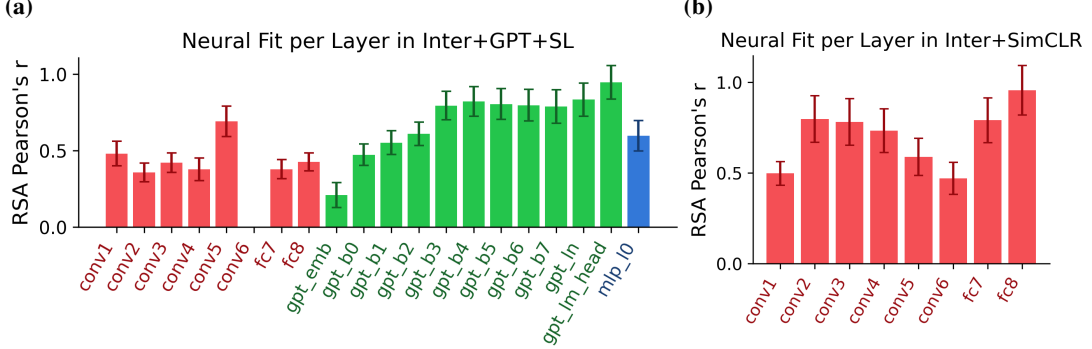


Figure A2: **Neural Fit Score per Model Layers** colored by **encoder**, **attender**, and **decoder**. No bar means the score is NaN for that layer. **(a)** Inter+GPT+SupervisedLearning is the model that scored the highest neural fit out of the supervised models. We observe that later GPT layers perform increasingly better. **(b)** The last fully-connected layer of Inter+SimCLR achieved the highest r value.

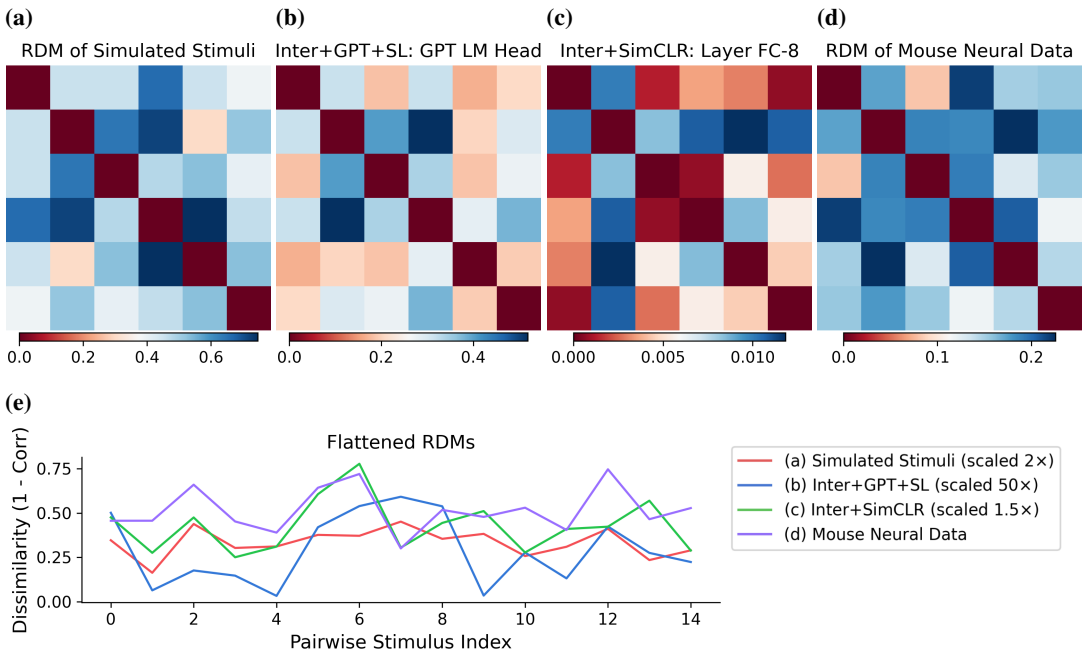


Figure A3: **Representational Dissimilarity Matrices** (RDM) for tactile data and neural evaluation. **(a)** RDM of the 6 simulated stimuli which is used as the model input in neural evaluation. **(b)** The GPT LM Head layer of Inter+GPT+SupervisedLearning is the supervised model with the highest neural fit score. **(c)** The last Fully-Connected layer in Inter+SimCLR achieves the highest neural fit score out of SSL models. **(d)** RDM performed on the 6 stimuli in the mice neural data. **(e)** A visualization of the flattened RDMs, scaled approximately to fit (RSA correlation does not take scale into account).